Thermodynamics of dipolar hard spheres with low-to-intermediate coupling constants

Ekaterina A. Elfimova and Alexey O. Ivanov
Institute of Mathematics and Computer Sciences, Ural Federal University, 51 Lenin Avenue, Ekaterinburg 620000, Russia

Philip J. Camp*
School of Chemistry, University of Edinburgh, West Mains Road, Edinburgh EH9 3JJ, Scotland
(Received 17 July 2012; published 23 August 2012)

The thermodynamic properties of the dipolar hard-sphere fluid are studied using theory and simulation. A new theory is derived using a convenient mathematical approximation for the Helmholtz free energy relative to that for the hard-sphere fluid. The approximation is designed to give the correct low-density virial expansion. New theoretical and numerical results for the fourth virial coefficient are given. Predictions of thermodynamic functions for dipolar coupling constants $\lambda = 1$ and 2 show excellent agreement with simulation results, even at the highest value of the particle volume fraction φ. For higher values of λ, there are deviations at high volume fractions, but the correct low-density behavior is retained. The theory is compared critically against the established thermodynamic perturbation theory; it gives significant improvements at low densities and is more convenient in terms of the required numerics. Dipolar hard spheres provide a basic model for ferrofluids, and the theory is accurate for typical experimental parameters $\lambda \lesssim 2$ and $\varphi \lesssim 0.1$. This is demonstrated explicitly by fitting osmotic equations of state for real ferrofluids measured recently by analytical centrifugation.

DOI: 10.1103/PhysRevE.86.021126 PACS number(s): 05.20.Jj, 05.70.Ce, 75.50.Mm, 64.10.+h

I. INTRODUCTION

The theory of fluids of polar molecules relies heavily on the use of simple molecular models [1]. The simplest model of a polar molecule is a dipolar hard sphere (DHS), this being a hard sphere of diameter σ bearing a permanent dipole moment $\boldsymbol{\mu}$ at its center. The interaction between two DHSs i and j is given by a sum of hard-sphere (HS) and dipolar (D) terms:

$$u_{ij} = u_{ij}^{\mathrm{HS}} + u_{ij}^{\mathrm{D}}. \tag{1}$$

The hard-sphere potential is

$$u_{ij}^{\mathrm{HS}} = \begin{cases} \infty & r_{ij} < \sigma \\ 0 & r_{ij} \geqslant \sigma \end{cases}, \tag{2}$$

and the dipolar potential is

$$u_{ij}^{\mathrm{D}} = \frac{\boldsymbol{\mu}_i \cdot \boldsymbol{\mu}_j}{r_{ij}^3} - \frac{3(\boldsymbol{\mu}_i \cdot \boldsymbol{r}_{ij})(\boldsymbol{\mu}_j \cdot \boldsymbol{r}_{ij})}{r_{ij}^5}, \tag{3}$$

where $\boldsymbol{r}_{ij}$ is the interparticle separation vector and $r_{ij} = |\boldsymbol{r}_{ij}|$. DHS fluids are useful models of ferrofluids: colloidal suspensions of ferromagnetic nanoparticles in liquids. Taking into account the nanoparticle polydispersity, it is possible to model very accurately the properties of real ferrofluids such as the magnetization curve [2,3]. The DHS fluid has been the subject of intense scrutiny over the years, in terms of its structure, phase behavior, and dynamics [4]. One of the longest outstanding questions is whether DHSs exhibit a vapor-liquid transition [5], from the early theoretical analysis by de Gennes and Pincus [6] through to the latest computer-simulation studies by Rovigatti *et al.* [7,8] The consensus from computer simulations is that there is no such transition in DHSs, but that it may arise in the presence of (small) additional interactions such as anisotropic repulsions [9], multipolar interactions [10], isotropic interactions [5,11–13], and interactions mediated by nonpolar particles [14]. Extrapolations of simulation data to the DHS limit yield estimates of the *putative* critical parameters; at the critical point, the dipolar coupling constant $\lambda = \beta\mu^2/\sigma^3 \simeq 6$ where $\beta = 1/k_{\mathrm{B}}T$, and the particle volume fraction $\varphi \simeq 0.05$ [5,10,13,14].

There are existing theories of DHS thermodynamics such as the mean spherical approximation (MSA) [15,16] and the thermodynamic perturbation theory (TPT) of Stell, Rasaiah, and Narang [17,18] as applied to DHSs by Rushbrooke, Stell, and Høye [19]. The relative performances of these theories have been neatly summarized by Henderson [20]. For the Helmholtz free energy at high density ($\varphi \simeq 0.47$) TPT predictions truncated at terms of order λ^2 and λ^3 bracket simulation results, but a simple Padé approximant (denoted here as Padé-TPT) that reproduces these terms [19] does well for λ as high as 4 [20,21]. The Padé-TPT and MSA theory do not give accurate results at low densities and in fact do not predict the virial coefficients accurately since they are low-order theories with respect to λ. The Padé-TPT and MSA theory predict critical points at $(\lambda,\varphi) = (3.58,0.0833)$ and $(4.44,0.0555)$, respectively [19]. Kalyuzhnyi and coworkers have developed a version of the TPT that accounts for the strong association between dipolar particles that sets in at $\lambda \gtrsim 4$ [22,23]. The theory is based on the identification of a central-force (CF) portion of the interaction potential responsible for particle association; in Ref. [23] the theory is called TPT-CF. TPT-CF gives an apparent DHS critical point at $(\lambda,\varphi) = (5.92,0.042)$ [23]. The theory is in accord with simulated equations of state at the high values of $\lambda = 4.50$ and 5.56 [24] inasmuch as the isotherms are supercritical ($T > T_{\mathrm{c}}$, $\lambda < \lambda_{\mathrm{c}}$), but quantitative agreement is lacking. The Padé-TPT and TPT-CF theories are very similar for low concentrations and $\lambda \lesssim 2$, where particle association is not pronounced.

*philip.camp@ed.ac.uk

Certainly the low-density behavior and virial coefficients are incorrect in both cases.

In recent experimental work, Luigjes *et al*. have obtained the equation of state (osmotic pressure Π as a function of φ) of colloidal suspensions of ferromagnetic nanoparticles (magnetite particles stabilized with oleic acid and dispersed in decalin) [25,26]. By analytical centrifugation of a suspension and measuring the concentration profile, the sedimentation equilibrium can be solved to yield Π over the concentration range $\varphi \lesssim 0.1$. By comparing the measured second virial coefficient B_2 to that for DHSs [27–29], an apparent value of λ may be obtained. For "large" nanoparticles with an average magnetic core diameter of 13.4 nm, the apparent value of λ lies in the range 2–3, with a mean value from different experiments (with different centrifuge rotor speeds and particle loadings) of $\lambda \simeq 2.2$.

The experimental studies have prompted a theoretical reinvestigation of the thermodynamic properties of DHSs at low volume fractions $\varphi \leqslant 0.1$ and with coupling constants of order 1. In this work a new theory is constructed based on the difference between the Helmholtz free energies of DHS and reference HS fluids. The only inputs of the theory are the differences between the first few DHS and HS virial coefficients, in practice computed as series expansions in λ. Explicit expressions for the free energy, chemical potential, and equation of state are presented. Comparison with new Monte Carlo (MC) simulation results shows that the theory works excellently over the whole fluid range of φ and up to $\lambda = 2$. Discrepancies set in at very high values of $\lambda = 3$ and 4; while the low-φ behavior is captured correctly (due to the correct virial coefficients being input), significant deviations are seen at higher concentrations. Overall the new theory is a significant improvement over the Padé-TPT at low volume fractions; while the latter is accurate at $\lambda = 1$ and 2, it does not give the correct virial coefficients, with the error becoming quite large at high values of λ. The new results should be of direct relevance to almost all real colloidal ferrofluids. Expressions for the equation of state and chemical potential are necessary for the study of phase equilibria, while the chemical potential is a fundamental input for the study of magnetophoresis, sedimentation, and gradient diffusion [30]. An advantage of the new theory is that the expressions are entirely analytic and simple, which facilitates fitting of experimental data. The new theory does not require any microscopic information for the reference HS system, whereas the coefficients appearing in TPT need to be computed from the HS radial distribution function at the required particle concentration. Hence, the new approach should be easily applied to other systems for which the thermodynamic properties of a related reference system are well known but the microscopic structure is not.

This article is arranged as follows. In Sec. II the theory and simulation methods are detailed, and new analytical and numerical results for the fourth virial coefficient of DHSs are presented. The main results are presented first as a comparison between theory and simulation for $1 \leqslant \lambda \leqslant 4$ (Sec. III A), and then as a comparison between theory and experiment for $\lambda \simeq 2.3$ (Sec. III B). The conclusions from the work are summarized in Sec. IV.

II. MODEL AND METHODS

A. Theory

Consider a fluid of N DHSs in a volume V at temperature T. The concentration is $\rho = N/V$, and the volume fraction is $\varphi = \rho v_0$ where $v_0 = \pi\sigma^3/6$ is the particle volume. The virial expansion for the Helmholtz free energy F is [31]

$$\frac{\beta F}{N} = \frac{\beta F^{\mathrm{id}}}{N} + \sum_{n=1}^{\infty} n^{-1} B_{n+1} \rho^n, \tag{4}$$

where F^{id} is the ideal-gas contribution and B_{n+1} is a temperature-dependent virial coefficient. The difference between virial expansions for the DHS fluid (F) and the HS fluid (F^{HS}) can be written as

$$\frac{\beta \Delta F}{N} = \frac{\beta (F - F^{\mathrm{HS}})}{N} = \sum_{n=1}^{\infty} n^{-1} G_{n+1} \varphi^n. \tag{5}$$

G_{n+1} is related to the virial coefficients by

$$G_{n+1} = \frac{B_{n+1} - B_{n+1}^{\mathrm{HS}}}{v_0^n}, \tag{6}$$

where B_{n+1} and B_{n+1}^{HS} are virial coefficients for the DHS and HS fluids, respectively. The second virial coefficient B_2 is known exactly in various forms [27,29] and as a series expansion in λ [28,32–34]:

$$B_2 = B_2^{\mathrm{HS}} \left[1 - \sum_{m=1}^{\infty} \frac{\lambda^{2m}}{(2m-1)[(2m+1)!!]^2} \sum_{r=0}^{m} \binom{2r}{r} \right] \tag{7}$$

$$= B_2^{\mathrm{HS}} - v_0 \left(\frac{4}{3}\lambda^2 + \frac{4}{75}\lambda^4 + \frac{116}{55125}\lambda^6 + \cdots \right), \tag{8}$$

$$B_2^{\mathrm{HS}} = 4 v_0. \tag{9}$$

$[(2m+1)!!$ means the product of all odd positive integers up to $(2m+1).]$ The third virial coefficient B_3 has been given as a series expansion in λ and from direct numerical computation [27,35]. The fourth virial coefficient B_4 seems not to have been given at all. The leading order expression for B_4 in terms of λ is derived in Appendix. The expansions for B_3 and B_4 are as follows:

$$\begin{aligned} B_3 = B_3^{\mathrm{HS}} - v_0^2 \Bigg[& \left(4\ln 2 + \frac{2}{3} \right) \lambda^2 - \frac{20}{9}\lambda^3 \\ & - \frac{1468}{15} \left(\ln 2 - \frac{1\,933\,981}{2\,818\,560} \right) \lambda^4 \Bigg] + 0.0424\lambda^5 \\ & + 0.00844\lambda^6 + 0.00391\lambda^7 - 0.000554\lambda^8 \\ & + 0.000401\lambda^9 - 0.000124\lambda^{10} + 0.0000356\lambda^{11} \\ & - 0.0000115\lambda^{12} + \cdots, \end{aligned} \tag{10}$$

$$B_3^{\mathrm{HS}} = 10 v_0^2, \tag{11}$$

$$B_4 = B_4^{\mathrm{HS}} - v_0^3 (2.901720\lambda^2 + \cdots), \tag{12}$$

$$B_4^{\mathrm{HS}} = \frac{v_0^3}{35} \left[-712 + \frac{219\sqrt{2}}{\pi} + \frac{4131}{\pi} \arccos\left(\frac{1}{\sqrt{3}} \right) \right]. \tag{13}$$

The numerical coefficients in Eq. (10) are taken from Ref. [35]; the numerical uncertainties in these figures are omitted, but

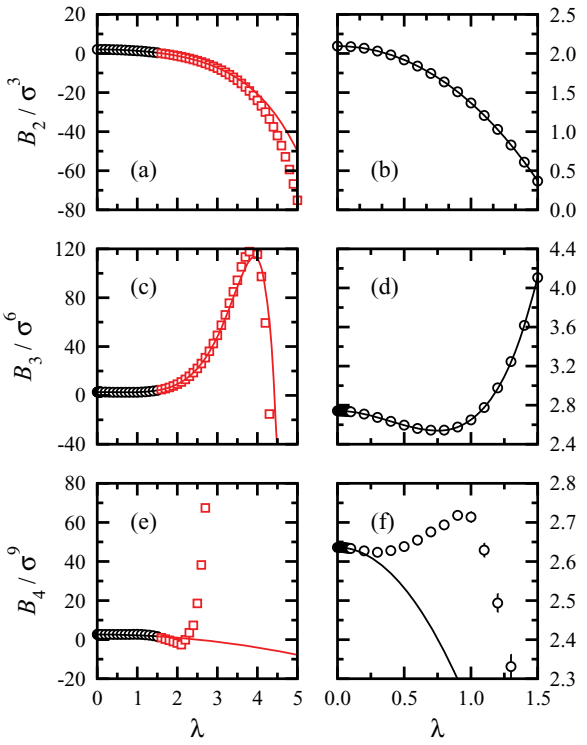

FIG. 1. (Color online) Virial coefficients for DHSs from numerical computation (points) and from expansions (lines) [Eqs. (8), (10), and (12)]: (a) and (b) B_2; (c) and (d) B_3; (e) and (f) B_4. Results are shown on two different scales, $0 \leqslant \lambda \leqslant 5$ and $0 \leqslant \lambda \leqslant 1.5$; the data represented by black circles in (a), (c), and (e) are shown on the expanded scale in (b), (d), and (f), respectively. Error bars are indicated in the numerical results for B_3 and B_4, but in most cases these are smaller than the symbol size.

they amount to less than 1% in each case. To test the expressions, B_3 and B_4 have been calculated in the range $0 \leqslant \lambda \leqslant 5$ by straightforward application of the Mayer-sampling method developed by Singh and Kofke [36]. In each calculation a total of 10^9 configurations was sampled with the acceptance rates for particle translations and rotations each set at 50%. The results are shown in Fig. 1 along with the exact result for B_2 and the expansions given above. For HSs ($\lambda = 0$) B_2, B_3, and B_4 are positive reflecting the purely repulsive interactions. With the introduction of dipolar interactions, B_2 decreases and eventually becomes negative beyond the "Boyle point" $\lambda \simeq 1.64$, signaling effective attractions between pairs of particles. B_3 initially decreases with increasing λ, but, as shown in Ref. [35], it exhibits a local minimum at $\lambda \simeq 0.75$ and a maximum at $\lambda \simeq 3.8$, and then decreases rapidly, becoming negative at $\lambda \gtrsim 4.3$. B_4 shows a very complex dependence on λ, with two minima (near $\lambda = 0.30$ and 2.10) and one local maximum (near $\lambda = 0.90$). Beyond $\lambda = 2.10$, B_4 increases rapidly and monotonically, and at $\lambda = 4$ is approximately equal to $2 \times 10^4 \sigma^9$ (not shown in Fig. 1). Overall, with λ increasing from 0 to 4, B_3 and B_4 signal changes in the collective interactions from increasing attraction to increasing repulsion. The expansion of B_2 up to λ^6 given in Eq. (8) converges rather rapidly, with the coefficients all of the same sign, and is quite accurate up to $\lambda = 4$ [28,29]. The expansion of B_3 in Eq. (10) exhibits coefficients of different sign and clearly does not converge very rapidly [35].

In a thermodynamic theory, one might strive to compute higher order virial coefficients to ever higher orders in λ, but this brute-force approach can lead to difficulties since the virial (and λ expansion) coefficients fluctuate in sign. Therefore, a polynomial expansion of the free energy might not be the best approach, since the result will depend sensitively on the terms of highest order in n and λ. Hence, it could be more effective to transform Eq. (5) back into a logarithmic form, such as in $\beta F/N = -\ln Q^{1/N}$ from which the virial expansion is derived in the first place. The advantage is that a logarithm of a polynomial is less sensitive to the truncation of the polynomial. An alternative to Eq. (5) is therefore

$$\frac{\beta \Delta F}{N} = -\ln\left[1 + \sum_{n=1}^{\infty} n^{-1} I_n \varphi^n\right], \tag{14}$$

where the minus sign at the front is important because the presence of cohesive dipolar interactions should give $\beta \Delta F < 0$. This means that the argument of the logarithm should always be greater than unity and hence there should be no danger of an accidental logarithmic divergence. Without the minus sign, the argument of the logarithm may accidentally approach zero, leading to a divergence. The coefficients I_n can be determined by matching terms between Eq. (5) and the Maclaurin series of Eq. (14). The first three coefficients are

$$I_1 = -G_2, \tag{15}$$

$$I_2 = -G_3 + G_2^2, \tag{16}$$

$$I_3 = -G_4 + \tfrac{3}{2} G_3 G_2 - \tfrac{1}{2} G_2^3. \tag{17}$$

Care has to be taken in the computation of these coefficients. B_2 and G_2 are computed using the expansion in Eq. (8) so that the theory is entirely analytic and can easily be fitted to experimental data, as demonstrated in Sec. III B. The expansion of B_3 and G_3 is known up to λ^{12}. Hence, I_2 should be computed to the same order, and so G_2 is included up to λ^6. B_4 and G_4 are known up to λ^2. Because $G_3 G_2$ and G_2^3 contribute only higher order terms, these should be neglected. Therefore, at the current level of approximation I_3 is truncated at λ^2, i.e., $I_3 \simeq -G_4$. The explicit expressions for I_1, I_2, and I_3 are as follows:

$$I_1 = \frac{4}{3}\lambda^2 + \frac{4}{75}\lambda^4 + \frac{116}{55\,125}\lambda^6, \tag{18}$$

$$\begin{aligned} I_2 = {} & \left(4\ln 2 + \frac{2}{3}\right)\lambda^2 - \frac{20}{9}\lambda^3 + \left(\frac{661\,727}{9600} - \frac{1468}{15}\ln 2\right)\lambda^4 \\ & - 0.155\lambda^5 + 0.111\lambda^6 - 0.0143\lambda^7 + 0.0105\lambda^8 \\ & - 0.00146\lambda^9 + 0.000677\lambda^{10} - 0.000130\lambda^{11} \\ & + 0.0000464\lambda^{12}, \end{aligned} \tag{19}$$

$$I_3 = 2.901720\lambda^2. \tag{20}$$

Given these expressions for I_n in terms of λ it is a simple matter to compute the Helmholtz free energy and the remaining thermodynamic functions, such as the pressure $P = -(\partial F/\partial V)_{N,T}$ and the chemical potential $\mu = (F + PV)/N$. Inserting the Carnahan-Starling equation of state for the HS

fluid [37], the properties of the DHS fluid are

$$\frac{\beta\Delta F}{N} = -\ln\left(1 + I_1\varphi + \frac{1}{2}I_2\varphi^2 + \frac{1}{3}I_3\varphi^3\right), \quad (21)$$

$$Z = \frac{\beta P}{\rho} = Z^{\rm HS} - \left(\frac{I_1\varphi + I_2\varphi^2 + I_3\varphi^3}{1 + I_1\varphi + \frac{1}{2}I_2\varphi^2 + \frac{1}{3}I_3\varphi^3}\right), \quad (22)$$

$$Z^{\rm HS} = \frac{1 + \varphi + \varphi^2 - \varphi^3}{(1-\varphi)^3}, \quad (23)$$

$$\beta\Delta\mu = \beta(\mu - \mu^{\rm HS}) = \frac{\beta\Delta F}{N} + Z - Z^{\rm HS}. \quad (24)$$

The new theory is compared to Padé-TPT [19]. In essence, the difference in Helmholtz free energy between DHSs and hard spheres at the same density and temperature is given by $\Delta F = \lambda^2 F_2/(1 - \lambda F_3/F_2)$, where F_2 and F_3 are the coefficients in the TPT of order λ^2 and λ^3, respectively. The coefficients are computed from the known radial distribution function for HSs, which is itself state dependent. Hence, TPT and its extensions [22,23] are more cumbersome than the new theory proposed here; both approaches require the thermodynamic functions of the reference system as input, but in the new theory, one just needs a few virial coefficients. In addition, the new approach is expected to give the correct low-density behavior, something that TPTs fail to treat correctly because of the low order in λ [20,29,35].

B. Simulations

Standard MC simulations were performed in the NPT ensemble using $N = 256$ particles in a cubic box with periodic boundary conditions [38]. The Ewald summation with conducting boundary conditions was used to handle the long-range dipolar interactions. One MC cycle consisted of, on average, N attempts at translating or rotating a randomly selected particle, and one attempt at altering the volume. Maximum translational, orientational, and volume displacement parameters were adjusted to give acceptance rates of approximately 20%, 50%, and 20%, respectively. For each state point, averages were calculated over 5×10^5 MC cycles after 1×10^5 cycles for equilibration. The Helmholtz free energy as a function of particle volume fraction φ was estimated by thermodynamic integration:

$$\frac{\beta F}{N} = \frac{\beta F^{\rm id}}{N} + \int_0^\varphi \left(\frac{Z-1}{\varphi}\right) d\varphi. \quad (25)$$

The Carnahan-Starling expression for the Helmholtz free energy of the HS fluid was used to obtain ΔF:

$$\frac{\beta F^{\rm HS}}{N} = \frac{\beta F^{\rm id}}{N} + \frac{\varphi(4-3\varphi)}{(1-\varphi)^2}. \quad (26)$$

The difference between chemical potentials of the DHS and HSs fluids $\beta\Delta\mu$ was computed using Eq. (24).

III. RESULTS

A. Comparison between theory and simulation for $1 \leqslant \lambda \leqslant 4$

Figure 2 shows $\beta\Delta F/N$ for $\lambda = 1$, 2, 3, and 4 from the new theory, Padé-TPT, and MC simulation. The new simulation results are compared with umbrella-sampling MC data from Ref. [39], which are for extremely small systems and without proper treatment of the long-range dipolar interactions. Nonetheless, the agreement between simulation results is excellent. The low-density virial expansion [Eq. (5)] clearly does not provide a reliable extrapolation to high densities, while the logarithmic expression [Eq. (21)] is far more accurate. The virial expansion is ignored henceforth. For $\lambda = 1$ and 2, the agreement between the theories and simulation is excellent. If anything, the new theory is slightly better at higher volume fractions, all the way up to $\varphi \simeq 0.4$. For $\lambda = 3$ and 4 the deviations between theory and simulation are significant, but in different ways. The Padé-TPT roughly tracks the simulation results, but the low-density behavior is inaccurate. The new theory, on the other hand, has the correct initial slope at low density and remains in good agreement with simulation up to $\varphi = 0.05$–0.1.

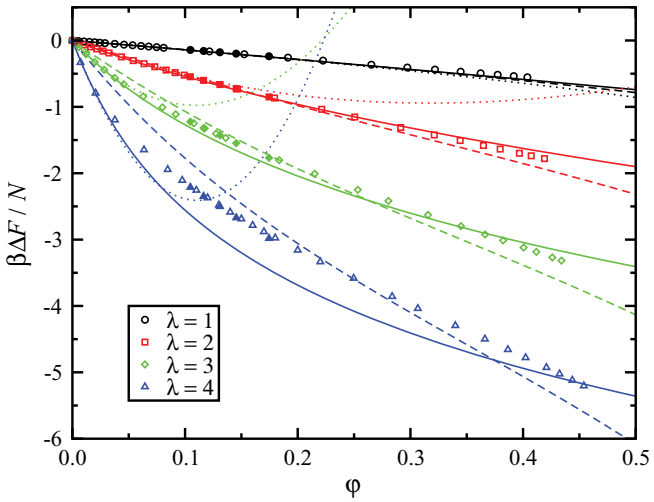

FIG. 2. (Color online) Difference between Helmholtz free energies of DHS and HS fluids $\beta\Delta F/N$ as a function of volume fraction φ for fluids with $\lambda = 1$ (black circles and lines), $\lambda = 2$ (red squares and lines), $\lambda = 3$ (green diamonds and lines), and $\lambda = 4$ (blue triangles and lines). The unfilled points are from the present MC simulations, the filled points are from umbrella-sampling MC simulations in Ref. [39], the dashed lines are from Padé-TPT, the solid lines are from the present theory [Eq. (21)], and the dotted lines are from the virial expansion [Eq. (5)].

A very similar picture emerges from the chemical potential $\beta\Delta\mu$ shown in Fig. 3. For $\lambda = 1$ there is very little to choose between the new theory and Padé-TPT in comparison to the simulation results; both are in excellent agreement with simulation results up to $\varphi \simeq 0.4$. For $\lambda = 2$ the agreement is good up to $\varphi \simeq 0.2$, and then the two theories part company. At $\lambda = 3$ and $\lambda = 4$ the the initial slopes are captured accurately by the new theory, while the Padé-TPT gets them completely wrong. The new theory remains accurate only as far as $\varphi \simeq 0.05$ at these high values of λ.

The equation of state is shown in Fig. 4 in the form of $\beta P v_0$ as a function of φ. For $\lambda = 1$ and 2 the new theory is in excellent agreement with the simulation results over the entire density range, although the scale obscures the low-density behavior, which will be elaborated upon below. The new theory and Padé-TPT appear to be of comparable accuracy. For $\lambda = 3$ and 4 both theories are inaccurate at high density

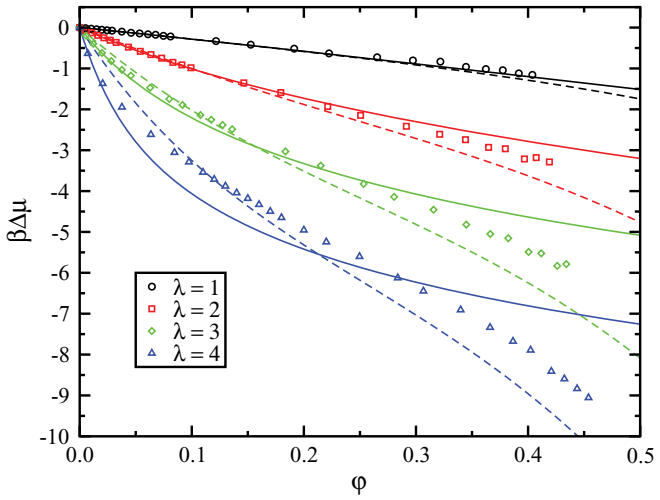

FIG. 3. (Color online) Difference between chemical potentials of DHS and HS fluids $\beta\Delta\mu$ as a function of volume fraction φ for DHS fluids with $\lambda = 1$ (black circles), $\lambda = 2$ (red squares), $\lambda = 3$ (green diamonds), and $\lambda = 4$ (blue triangles). The points are from MC simulations, the dashed lines are from Padé-TPT, and the solid lines are from the present theory.

$\varphi \gtrsim 0.2$. The Padé-TPT critical point is at $\lambda = 3.58$, and since $\lambda = 4$ corresponds to a subcritical isotherm ($T < T_c$), there is a "flattening" of the equation of state and hence a deviation from the simulation results. In the new theory, solving the simultaneous equations $(\partial P/\partial V) = 0$ and $(\partial^2 P/\partial V^2) = 0$ yields the critical point at $(\lambda,\varphi) = (3.64, 0.0493)$, and so $\lambda = 4$ corresponds to a subcritical isotherm here as well.

The relative performance of the theories in predicting the equation of state, particularly at low density, is clarified in Figs. 5 and 6. The compressibility factor Z in Fig. 5 highlights the shortcomings of the both the new theory and Padé-TPT, since at $\lambda = 4$ there are significant negative deviations even at low densities in the region of $\varphi \simeq 0.1$. For $\lambda = 1$, 2, and 3, however, the agreement between both theories and simulation

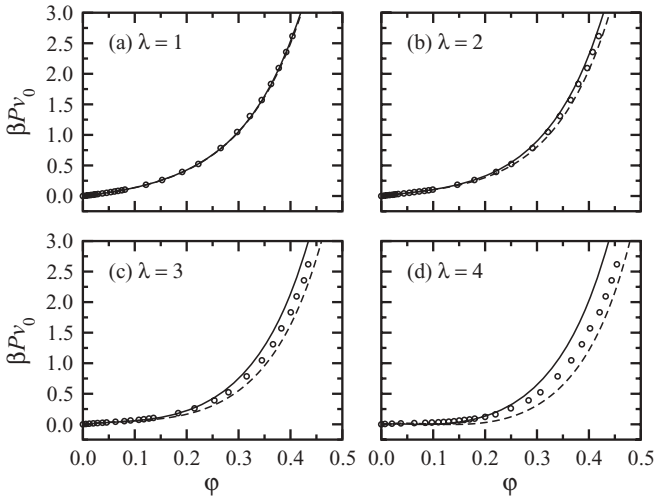

FIG. 4. The equation of state for DHS fluids with (a) $\lambda = 1$, (b) $\lambda = 2$, (c) $\lambda = 3$, and (d) $\lambda = 4$. The points are from MC simulations, the dashed lines are from Padé-TPT, and the solid lines are from the present theory.

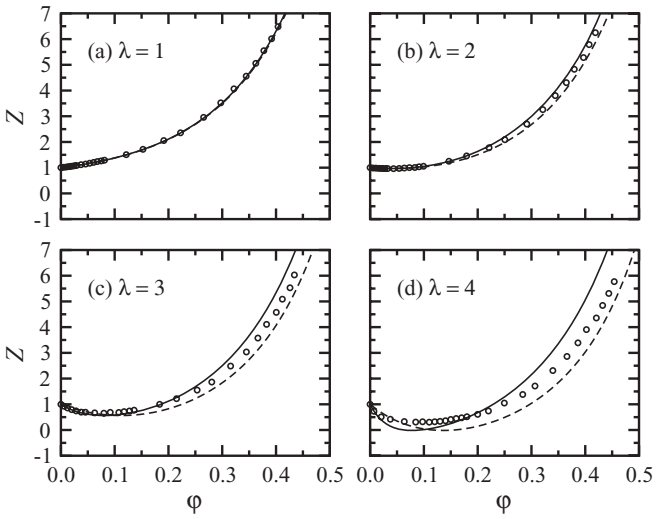

FIG. 5. The compressibility factor $Z = \beta P/\rho$ as a function of volume fraction φ for DHS fluids with (a) $\lambda = 1$, (b) $\lambda = 2$, (c) $\lambda = 3$, and (d) $\lambda = 4$. The points are from MC simulations, the dashed lines are from Padé-TPT, and the solid lines are from the present theory.

is rather good. A closer inspection of the low-density behavior, however, shows up some significant differences. In Fig. 6 we plot the quantity $(Z-1)/B_2\rho$ where B_2 is the *exact* value. At low density

$$\frac{Z-1}{B_2\rho} \approx 1 + \left(\frac{B_3}{B_2 v_0}\right)\varphi, \tag{27}$$

and so the limiting slope and intercept predicted by theory should show up inaccuracies in the expressions for B_2 and B_3. In all cases, the new theory outperforms the Padé-TPT because of the accurate representations of B_2 and B_3 given in Eqs. (8) and (10), respectively. At higher densities, both theories are of comparable accuracy.

The reasons for the relative performance of the theories are quite clear. The Padé-TPT contains terms only up to λ^3, and

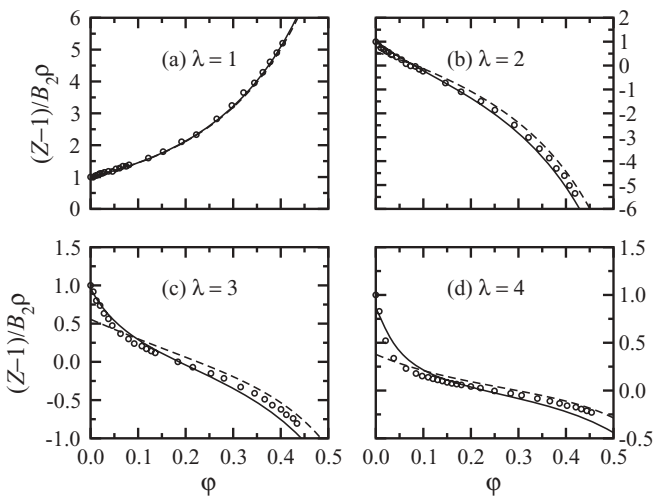

FIG. 6. $(Z-1)/B_2\rho$ as a function of volume fraction φ for DHS fluids with (a) $\lambda = 1$, (b) $\lambda = 2$, (c) $\lambda = 3$, and (d) $\lambda = 4$. The points are from MC simulations, the dashed lines are from Padé-TPT, and the solid lines are from the present theory.

this truncation is particularly serious for the second and third virial coefficients, which govern the low-density behavior of the properties under consideration. The new theory contains accurate representations of B_2 and B_3 by construction, and hence the low-density behavior is captured correctly.

B. Comparison between theory and experiment at $\lambda \simeq 2$

In Refs. [25,26], Luigjes *et al.* present measurements of the osmotic pressure Π as a function of ferrofluid volume fraction φ from analytical centrifugation experiments. The compressibility factor $Z = \beta\Pi/\rho$ was found to be a roughly linear decreasing function of volume fraction $\varphi \lesssim 0.1$ and was fitted using the second-virial expression $Z \approx 1 + B_2\rho$. An apparent value of λ can be obtained from the fitted value of B_2. Measurements were taken using two different centrifuges and at different rotor speeds. For 13.4 nm particles, an average value of $\lambda \simeq 2.2$ was obtained. Note that B_2 is a rapidly decreasing function of λ. Hence, a small deviation in the measured value of B_2 lead to a large change in the apparent value of λ.

Figure 7 shows some of the experimental data of Luigjes *et al.* in the form of the equation of state ($\beta\Pi v_0$ versus φ). The data were analyzed in the range $\varphi \leqslant 0.04$ using Eq. (22)

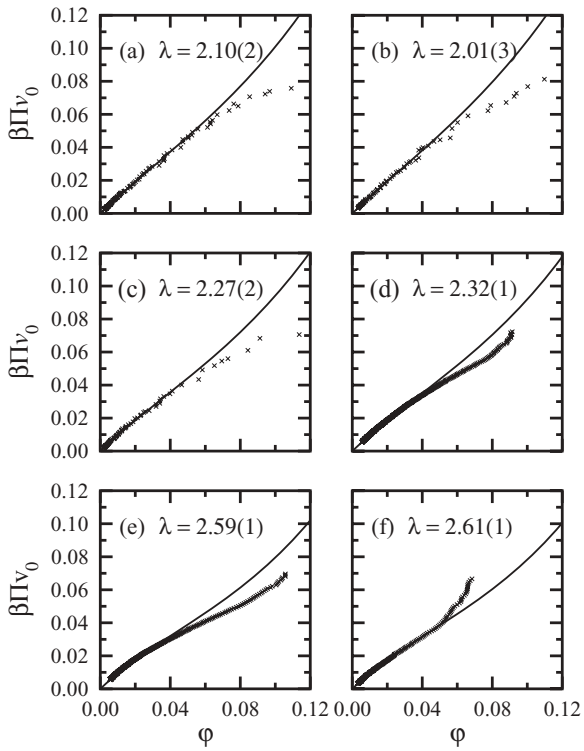

FIG. 7. The equation of state from experiment (crosses) and theory with the indicated values of λ (solid lines); the digits in brackets are estimated fitting uncertainties in the final significant figures. The experimental data taken with different equipment, centrifuge rotor speeds, and particle loadings are as given in Ref. [26]. (a)–(c) Beckman analytical centrifuge: (a) 1200rpm and 36 gL^{-1}; (b) 1400 rpm and 36 gL^{-1}; (c) 1600 rpm and 36 gL^{-1}. (d)–(f) LUMifuge low-speed centrifuge: (d) 500 rpm and 134 gL^{-1}; (e) 625 rpm and 134 gL^{-1}; (f) 1000 rpm and 134 gL^{-1}.

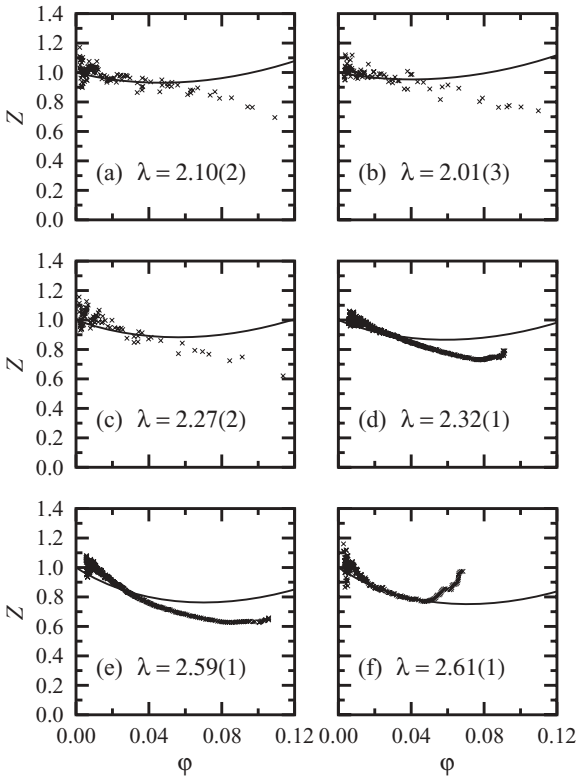

FIG. 8. The compressibility factor $Z = \beta\Pi/\rho$ as a function of volume fraction φ from experiment (crosses) and theory with the indicated values of λ (solid lines); the digits in brackets are estimated fitting uncertainties in the final significant figures. The experimental details are the same as those in Fig. 7.

and by fitting λ directly. The apparent values of λ are given in Fig. 7, lie in the range 2.0–2.6, and have an average value of about 2.3. These numbers are in excellent agreement with those reported by Luigjes *et al.* given the likely experimental uncertainties.

Figure 8 shows the compressibility factor $Z = \beta\Pi/\rho$ along with the theoretical curves for the values of λ determined above, to show consistency. (Fitting to Z leads to values of λ about 5% higher than those determined above.) For these values of λ, the DHS equation of state shows more curvature than that seen in experiments. This is not due to the accuracy of theory, because the comparison with simulation results shows that it is reliable in the region $\varphi \lesssim 0.1$ and $\lambda \simeq 2$. The reasons for the discrepancy are not known, but they might arise from describing a complex colloidal system with as simple a model as monodisperse DHSs.

IV. CONCLUSIONS

A new thermodynamic theory of dipolar hard-sphere fluids has been derived by representing the free energy with respect to that of the hard-sphere fluid by a logarithmic equation. The argument of the logarithm is a polynomial expansion in density with coefficients chosen to give the first few terms in the conventional virial expansion. The new theory has been compared to existing thermodynamic perturbation theory and the results from computer simulations. The comparison

has been made in terms of the Helmholtz free energy, the chemical potential, and the equation of state. For low values of the dipolar coupling constant ($\lambda = 1$ and 2), the agreement between the new theory and simulation is excellent. Deviations set in for stronger dipolar coupling ($\lambda = 3$ and 4) and at high density ($\varphi \gtrsim 0.1$), but the theory retains the correct low-density behavior by construction. The thermodynamic perturbation theory is competitive at high densities, but for strong dipolar coupling, the predicted low-density behavior is in significant error. The reasons for this arise primarily from the thermodynamic perturbation theory being truncated at low order in the dipolar coupling constant with higher order terms accounted for in an approximate Padé summation.

From a practical point of view, the new theory is extremely simple, and the basic approach may be applied to other situations where the properties of a reference system are known. With just a few low-order virial coefficients, the properties at low and high density may be predicted. By contrast, the expansion coefficients in thermodynamic perturbation theory are obtained by integrals over the state-dependent radial distribution function of the reference system. This is a cumbersome process, and in general the microscopic properties of the reference system might not even be known. Examples of systems to which the new theory could be applied, starting from the hard-sphere free energy, include the square-well fluid [40], patchy colloids [41], hard ellipsoids [42], charged hard spheres [43], and systems with higher multipolar moments. More realistic atomistic models based on Lennard-Jones and electrostatic interactions might also be tackled, using the Lennard-Jones fluid as a reference system.

The new theory has been used to fit osmotic equations of state for real ferrofluids over the density range $\varphi \leqslant 0.04$. The values of the dipolar coupling constant ($\lambda \simeq 2.3$) are in good agreement with those extracted by other methods. The accuracy of the theory in the relevant experimental regime ($\varphi \lesssim 0.1$ and $\lambda \lesssim 2$) has been demonstrated. It is hoped that the explicit results of this work provide a convenient means of computing the thermodynamic properties of model polar fluids and real ferrofluids.

ACKNOWLEDGMENTS

The authors thank Ben Erné, Bob Luigjes, and Albert Philipse (Utrecht) for supplying the experimental data and for motivating the current work. E.A.E. and A.O.I. gratefully acknowledge grants from the Ministry of Education and Science of the Russian Federation and the Russian Foundation for Basic Research. P.J.C. thanks the Ural Federal University for supporting a collaborative visit to Ekaterinburg.

APPENDIX: CALCULATION OF B_4

In the absence of an applied field, the fourth virial coefficient is given by [31]

$$B_4 = -\frac{1}{8V}\int\!\!\int\!\!\int\!\!\int (3 f_{12} f_{23} f_{34} f_{14} + 6 f_{12} f_{23} f_{34} f_{14} f_{13} + f_{12} f_{23} f_{34} f_{14} f_{13} f_{24})\, d1\, d2\, d3\, d4, \tag{A1}$$

where $\int di = (4\pi)^{-1} \int d\boldsymbol{r}_i \int \mathrm{d}\boldsymbol{\Omega}_i$ represents, for particle i ($i = 1,2,3,4$), an integration over the position vector $\boldsymbol{r}$ and an average over the orientation unit vector $\boldsymbol{\Omega}$. The Mayer f function between particles i and j is $f_{ij} = \exp(-\beta u_{ij}) - 1$ and can be decomposed in to hard-sphere (HS) and dipolar (D) f functions according to the potentials in Eqs. (2) and (3):

$$f_{ij} = f_{ij}^{\mathrm{HS}} + \left(f_{ij}^{\mathrm{HS}} + 1\right) f_{ij}^{\mathrm{D}}. \tag{A2}$$

The dipolar f function f_{ij}^{D} is expanded in terms of λ:

$$f_{ij}^{\mathrm{D}} = \sum_{l=1}^{\infty} \frac{\lambda^l}{l!} \left(\frac{-\beta u_{ij}^{\mathrm{D}}}{\lambda}\right)^l. \tag{A3}$$

Inserting Eqs. (A2) and (A3) in to the definition of B_4 yields an expansion in λ. Terms of order λ disappear because $\int\!\!\int u_{12}^{\mathrm{D}} d\boldsymbol{\Omega}_1\, d\boldsymbol{\Omega}_2 = 0$ [44]. To order λ^2 the expansion is

$$G_4 = \frac{B_4 - B_4^{\mathrm{HS}}}{v_0^3} = -\lambda^2 (\Gamma_1 + \Gamma_2 + \Gamma_3 + \Gamma_4) + \cdots, \tag{A4}$$

where Γ_1 to Γ_4 correspond to topologically distinct diagrams. Taking particle 1 to be at the origin, these coefficients are

$$\Gamma_1 = \frac{3}{4v_0^3}\int\!\!\int\!\!\int \left(f_{12}^{\mathrm{HS}} + 1\right) g_{12}^{\mathrm{D}} f_{23}^{\mathrm{HS}} f_{34}^{\mathrm{HS}} f_{14}^{\mathrm{HS}}\, d\boldsymbol{r}_2\, d\boldsymbol{r}_3\, d\boldsymbol{r}_4, \tag{A5}$$

$$\Gamma_2 = \frac{3}{2v_0^3}\int\!\!\int\!\!\int \left(f_{12}^{\mathrm{HS}} + 1\right) g_{12}^{\mathrm{D}} f_{23}^{\mathrm{HS}} f_{34}^{\mathrm{HS}} f_{14}^{\mathrm{HS}} f_{13}^{\mathrm{HS}}\, d\boldsymbol{r}_2\, d\boldsymbol{r}_3\, d\boldsymbol{r}_4, \tag{A6}$$

$$\Gamma_3 = \frac{3}{8v_0^3}\int\!\!\int\!\!\int f_{12}^{\mathrm{HS}} f_{23}^{\mathrm{HS}} f_{34}^{\mathrm{HS}} f_{14}^{\mathrm{HS}} \left(f_{13}^{\mathrm{HS}} + 1\right) g_{13}^{\mathrm{D}}\, d\boldsymbol{r}_2\, d\boldsymbol{r}_3\, d\boldsymbol{r}_4, \tag{A7}$$

$$\Gamma_4 = \frac{3}{8v_0^3}\int\!\!\int\!\!\int \left(f_{12}^{\mathrm{HS}} + 1\right) g_{12}^{\mathrm{D}} f_{23}^{\mathrm{HS}} f_{34}^{\mathrm{HS}} f_{14}^{\mathrm{HS}} f_{13}^{\mathrm{HS}} f_{24}^{\mathrm{HS}} \times d\boldsymbol{r}_2\, d\boldsymbol{r}_3\, d\boldsymbol{r}_4, \tag{A8}$$

where g_{12}^{D} is given by

$$g_{12}^{\mathrm{D}} = \frac{1}{(4\pi)^2}\int\!\!\int \left(\frac{-\beta u_{12}^{\mathrm{D}}}{\lambda}\right)^2 d\boldsymbol{\Omega}_1\, d\boldsymbol{\Omega}_2 = \frac{2}{3x_{12}^6} \tag{A9}$$

and is a function only of the reduced distance $x_{12} = |\boldsymbol{r}_2 - \boldsymbol{r}_1|/\sigma$ of particle 2 from particle 1. There is an equivalent expression for g_{13}^{D}. The remaining integrations are relatively straightforward and were first considered by Nijboer and Van Hove in the calculation of the third virial coefficient for hard spheres [45]. In each case, integrations over the position vectors $\boldsymbol{r}_3$ or $\boldsymbol{r}_4$ (or $\boldsymbol{r}_2$ and $\boldsymbol{r}_4$) yield functions only of x_{12} (or x_{13}); these are denoted by w_1 to w_4. The coefficients Γ_1 to Γ_4 can then be determined by direct integration with respect to $\boldsymbol{r}_2$ (or $\boldsymbol{r}_3$). All of the w functions given below are equal to

zero outside of the ranges indicated:

$$w_1(x_{12}) = \frac{\left(f_{12}^{\rm HS}+1\right)}{v_0^2}\iint f_{23}^{\rm HS} f_{34}^{\rm HS} f_{14}^{\rm HS}\, d\boldsymbol{r}_3\, d\boldsymbol{r}_4, \quad w_1(x) = -\frac{x^6}{35} + \frac{9x^4}{5} - 6x^3 - 9x^2 + \frac{324x}{5} - 81 + \frac{486}{35x}(1 \leqslant x < 3),$$

$$\Gamma_1 = \frac{3}{4v_0}\int g_{12}^{\rm D} w_1(x_{12})\, d\boldsymbol{r}_2 = \frac{1504}{35} - 72\ln 3. \tag{A10}$$

$$w_2(x_{12}) = \frac{\left(f_{12}^{\rm HS}+1\right)}{v_0^2}\iint f_{23}^{\rm HS} f_{34}^{\rm HS} f_{14}^{\rm HS} f_{13}^{\rm HS}\, d\boldsymbol{r}_3\, d\boldsymbol{r}_4, \quad w_2(x) = \frac{x^6}{35} - \frac{9x^4}{5} + 6x^3 + 9x^2 - \frac{291x}{5} + 64 - \frac{324}{35x}(1 \leqslant x < 2),$$

$$\Gamma_2 = \frac{3}{2v_0}\int g_{12}^{\rm D} w_2(x_{12})\, d\boldsymbol{r}_2 = 144\ln 2 - \frac{4303}{70}. \tag{A11}$$

$$w_3(x_{13}) = \frac{\left(f_{13}^{\rm HS}+1\right)}{v_0^2}\iint f_{12}^{\rm HS} f_{23}^{\rm HS} f_{34}^{\rm HS} f_{14}^{\rm HS}\, d\boldsymbol{r}_2\, d\boldsymbol{r}_4, \quad w_3(x) = \left(8 - 6x + \frac{x^3}{2}\right)^2 (1 \leqslant x < 2),$$

$$\Gamma_3 = \frac{3}{8v_0}\int g_{13}^{\rm D} w_3(x_{13})\, d\boldsymbol{r}_3 = 48\ln 2 - \frac{57}{2}. \tag{A12}$$

$$\begin{aligned}
\frac{\left(f_{12}^{\rm HS}+1\right)}{v_0^2}\iint f_{23}^{\rm HS} f_{34}^{\rm HS} f_{14}^{\rm HS} f_{13}^{\rm HS} f_{24}^{\rm HS}\, d\boldsymbol{r}_3\, d\boldsymbol{r}_4 &= \frac{\left(f_{12}^{\rm HS}+1\right)}{v_0^2}\iint f_{23}^{\rm HS}\left(f_{34}^{\rm HS}+1\right) f_{14}^{\rm HS} f_{13}^{\rm HS} f_{24}^{\rm HS}\, d\boldsymbol{r}_3\, d\boldsymbol{r}_4 \\
&\quad - \frac{\left(f_{12}^{\rm HS}+1\right)}{v_0^2}\iint f_{23}^{\rm HS} f_{14}^{\rm HS} f_{13}^{\rm HS} f_{24}^{\rm HS}\, d\boldsymbol{r}_3\, d\boldsymbol{r}_4 \\
&= w_4(x_{12}) - w_3(x_{12}), \\
w_4(x) &= \left(-\frac{27x^4}{70} + \frac{123x^2}{35}\right)\sqrt{3-x^2} + \left(-\frac{276x}{5} + \frac{1296}{35x}\right)\arccos\left[\frac{x}{\sqrt{3(4-x^2)}}\right] \\
&\quad + \left(\frac{27x^6}{140} - \frac{12x^4}{5} + 18x^2 + \frac{24x}{5} - \frac{324}{35x}\right)\arccos\left[\frac{x^2+x-3}{\sqrt{3(4-x^2)}}\right] \\
&\quad + \left(\frac{27x^6}{140} - \frac{12x^4}{5} + 18x^2 - \frac{24x}{5} + \frac{324}{35x}\right)\arccos\left[\frac{-x^2+x+3}{\sqrt{3(4-x^2)}}\right](1 \leqslant x < \sqrt{3}), \\
\Gamma_4 &= \frac{3}{8v_0}\int g_{12}^{\rm D}\left[w_4(x_{12}) - w_3(x_{12})\right] d\boldsymbol{r}_2 \simeq 0.68861033 - \Gamma_3.
\end{aligned} \tag{A13}$$

Combining Γ_1 to Γ_4 with Eq. (A4) gives

$$G_4 \simeq -2.901720\lambda^2, \tag{A14}$$

which is equivalent to Eq. (12).

[1] C. G. Gray and K. E. Gubbins, *Theory of Molecular Fluids. Volume 1: Fundamentals* (Clarendon, Oxford, 1984).

[2] A. O. Ivanov, S. S. Kantorovich, E. N. Reznikov, C. Holm, A. F. Pshenichnikov, A. V. Lebedev, A. Chremos, and P. J. Camp, Phys. Rev. E **75**, 061405 (2007).

[3] A. O. Ivanov, S. S. Kantorovich, E. N. Reznikov, C. Holm, A. F. Pshenichnikov, A. V. Lebedev, A. Chremos, and P. J. Camp, Magnetohydrodynamics **43**, 393 (2007).

[4] P. I. C. Teixeira, J. M. Tavares, and M. M. Telo da Gama, J. Phys.: Condens. Matter **12**, 411R (2000).

[5] G. Ganzenmüller, G. N. Patey, and P. J. Camp, Mol. Phys. **107**, 403 (2009).

[6] P. G. de Gennes and P. A. Pincus, Phys. Kondens. Materie **11**, 189 (1970).

[7] L. Rovigatti, J. Russo, and F. Sciortino, Phys. Rev. Lett. **107**, 237801 (2011).

[8] L. Rovigatti, J. Russo, and F. Sciortino, Soft Matter **8**, 6310 (2012).

[9] S. C. McGrother and G. Jackson, Phys. Rev. Lett. **76**, 4183 (1996).

[10] G. Ganzenmüller and P. J. Camp, J. Chem. Phys. **126**, 191104 (2007).

[11] I. Szalai, D. Henderson, D. Boda, and K.-Y. Chan, J. Chem. Phys. **111**, 337 (1999).

[12] Y. V. Kalyuzhnyi, I. A. Protsykevytch, G. Ganzenmüller, and P. J. Camp, Europhys. Lett. **84**, 26001 (2008).

[13] M. Martín-Betancourt, J. M. Romero-Enrique, and L. F. Rull, Mol. Phys. **107**, 563 (2009).

[14] N. G. Almarza, E. Lomba, C. Martín, and A. Gallardo, J. Chem. Phys. **129**, 234504 (2008).
[15] M. S. Wertheim, J. Chem. Phys. **55**, 4291 (1971).
[16] G. Nienhuis and J. M. Deutch, J. Chem. Phys. **56**, 5511 (1972).
[17] G. Stell, J. C. Rasaiah, and H. Narang, Mol. Phys. **23**, 393 (1972).
[18] G. Stell, J. C. Rasaiah, and H. Narang, Mol. Phys. **27**, 1393 (1974).
[19] G. S. Rushbrooke, G. Stell, and J. S. Høye, Mol. Phys. **26**, 1199 (1973).
[20] D. Henderson, Condens. Matter Phys. **14**, 33001 (2011).
[21] L. Verlet and J.-J. Weis, Mol. Phys. **28**, 665 (1974).
[22] Y. V. Kalyuzhnyi and G. Stell, Mol. Phys. **78**, 1247 (1993).
[23] Y. V. Kalyuzhnyi, I. A. Protsykevytch, and P. T. Cummings, Europhys. Lett. **80**, 56002 (2007).
[24] J.-M. Caillol, J. Chem. Phys. **98**, 9835 (1993).
[25] B. Luigjes, D. M. E. Thies-Weesie, A. P. Philipse, and B. H. Erné, J. Phys.: Condens. Matter **24**, 245103 (2012).
[26] B. Luigjes, D. M. E. Thies-Weesie, B. H. Erné, and A. P. Philipse, J. Phys.: Condens. Matter **24**, 245104 (2012).
[27] C. G. Joslin, Mol. Phys. **42**, 1507 (1981).
[28] A. P. Philipse and B. W. M. Kuipers, J. Phys.: Condens. Matter **22**, 325104 (2010).
[29] D. Henderson, J. Chem. Phys. **135**, 044514 (2011).
[30] A. F. Pshenichnikov, E. A. Elfimova, and A. O. Ivanov, J. Chem. Phys. **134**, 184508 (2011).
[31] J.-P. Hansen and I. R. McDonald, *Theory of Simple Liquids*, 3rd ed. (Academic Press, London, 2006).
[32] W. H. Keesom, Comm. Phys. Lab. Leiden, Supp. B **24** (1912).
[33] W. H. Keesom, Phys. Z. **22**, 129 (1921).
[34] W. H. Keesom, Phys. Z. **22**, 643 (1921).
[35] C. Joslin and S. Goldman, Mol. Phys. **79**, 499 (1993).
[36] J. K. Singh and D. A. Kofke, Phys. Rev. Lett. **92**, 220601 (2004).
[37] N. F. Carnahan and K. E. Starling, J. Chem. Phys. **51**, 635 (1969).
[38] M. P. Allen and D. J. Tildesley, *Computer Simulation of Liquids* (Clarendon Press, Oxford, 1987).
[39] K. C. Ng, J. P. Valleau, G. M. Torrie, and G. N. Patey, Mol. Phys. **38**, 781 (1979).
[40] E. Schöll-Paschinger, A. L. Benavides, and R. Castañeda-Priego, J. Chem. Phys. **123**, 234513 (2005).
[41] C. Gögelein, F. Romano, F. Sciortino, and A. Giacometti, J. Chem. Phys. **136**, 094512 (2012).
[42] M. Dennison and A. J. Masters, Phys. Rev. E **84**, 021709 (2011).
[43] P. J. Camp and G. N. Patey, J. Chem. Phys. **111**, 9000 (1999).
[44] E. A. Elfimova and A. O. Ivanov, J. Exp. Theor. Phys. **111**, 146 (2010).
[45] B. R. A. Nijboer and L. Van Hove, Phys. Rev. **85**, 777 (1952).